Macromolecules

Article

pubs.acs.org/Macromolecules

Superior Chemotherapeutic Benefits from the Ruthenium-Based Anti-Metastatic Drug NAMI-A through Conjugation to Polymeric Micelles

Bianca M. Blunden,[†,‡] Aditya Rawal,[§] Hongxu Lu,[†] and Martina H. Stenzel[†,*]

[†]Centre for Advanced Macromolecular Design, University of New South Wales, Sydney, NSW 2052, Australia

[‡]Cooperative Research Centre (CRC) for Polymers, 8 Redwood Drive, Notting Hill, Victoria 3618, Australia

[§]NMR Facility, Mark Wainwright Analytical Centre, University of New South Wales, Sydney, NSW 2052, Australia

Supporting Information

ABSTRACT: Macromolecular ruthenium complexes are a promising avenue to better, and more selective, chemotherapeutics. NAMI-A is a ruthenium(III) drug in Phase II clinical trials that has low cytotoxicity and is inactive against primary tumors. However, it displays both antiangiogenic and anti-invasive properties and has been shown to specifically target tumor metastases, preventing both development and growth. To increase the cytotoxicity and cell uptake of this promising drug, we designed a biocompatible amphiphilic block copolymer capable of self-assembling into polymeric micelles. An appropriate method for the synthesis of a macromolecular NAMI-A drug was identified—the polymerization of vinyl imidazole and subsequent addition of a ruthenium(III) precursor complex. The cytotoxicity of these polymeric moieties was tested on ovarian cancer A2780 and Ovcar-3 and pancreatic AsPC-1 cancer cell lines. On average, across the tested cell lines, a 1.5 times increase in toxicity was found for the NAMI-A copolymer micelles when compared to the NAMI-A molecule. Furthermore, the antimetastatic potential was assessed by evaluating the inhibitory effects on the migration and invasion of cells against three cell lines characterized by differing degrees of malignancy (MDA-MB-231 > MCF-7 > CHO). The NAMI-A micelles were shown to have an improved antimetastatic potential in comparison to NAMI-A.

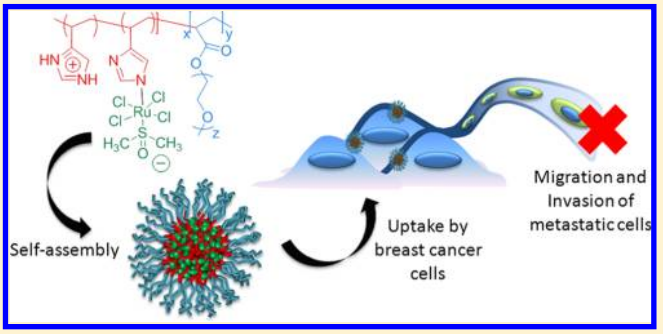

INTRODUCTION

Over the past 25 years, numerous ruthenium complexes have been investigated for medicinal applications. Two Ru^{III} compounds have entered phase II clinical trials: KP1019 has been shown to have anticancer activity while NAMI-A is an antimetastatic agent. Antimetastatic agents are extremely important in the treatment of cancer, since the majority of cancer patients die from these secondary cancers.

NAMI-A has low cytotoxicity and is inactive against primary tumors and thus failed the usual screens of putative anticancer agents.[1] However, it has been shown to specifically target tumor metastases,[2−4] preventing both development and growth,[1,3,5] and has significantly greater activity than Cisplatin on these cell types.[6] The NAMI-A effect appears to be independent of the type of primary tumor or the stage of growth of metastases.[3] It displays both antiangiogenic and anti-invasive properties on tumor cells and blood vessels.[1] It modifies important parameters of the metastasis such as tumor invasion, matrix metallo-proteinases activity, and cell cycle progression.[7]

However, the hydrolytic stability of NAMI-A in phosphate buffer (pH 7.4) at 37 °C is a limiting factor for administration since it has a half-life of less than 30 min. Thus, NAMI-A is administered with a physiological concentration of sodium chloride to enhance the stability in the infusion solution, when given to patients.[8]

It has previously been demonstrated that the therapeutic benefits of anticancer drugs, for example platinum-centered,[9] gold-centered,[10] or ruthenium-centered,[11,12] can be enhanced by encapsulation in, or conjugation to, a polymer matrix. The surrounding polymer protects the drug, increases solubility and often increases cell uptake efficiency due to the cell entry process being altered from a diffusion mechanism to endocytosis.[13] The creation of a drug carrier in the nanosize range enables fast endocytosis. Micelles present a unique size that leads to increased circulation times,[14] and the potential to exploit the EPR effect,[15] which are important properties for therapeutic moieties. Covalent attachment of a therapeutic agent is a useful avenue to delay drug release until the micelle reaches a target site.[16] Micelles, wherein a drug is covalently bound have been investigated, for example, PEG-*b*-poly(ε-caprolactone) with chemically conjugated docetaxel[17] and a

Received: October 9, 2013
Revised: February 6, 2014

   dx.doi.org/10.1021/ma402078d | *Macromolecules* XXXX, XXX, XXX−XXX

number of poly(ethylene oxide) based polymers containing cisplatin.[18−24]

NAMI-A comprises an imidazole ligand and counterion. The imidazole ring is biocompatible, antimicrobial, and anti-inflammatory and can regulate blood pressure.[25] It has many uses, which often center around its ability to bond to metals as a ligand and its ability to hydrogen bond with drugs and proteins.[25] Imidazoles also play a vital role in the inhibition of post-translational farnesylation—a key step for RAS proteins that influence cancer proliferation.[25]

Importantly, for this work, the imidazole ligand provides an avenue for polymerization. Poly(vinyl imidazole)s have long been investigated for their use as catalysts, pH-sensitive DNA carriers,[26] complex coacervates,[27] nonviral gene delivery therapeutics,[28,29] and oxygen transport membranes.[25] Also, imidazolium salts are used to extract metal ions from aqueous media,[30] coat metal nanoparticles, dissolve carbohydrates, and create polyelectrolyte brushes on surfaces.[25] Imidazolium analogues offer electrostatic interactions, aggregation, and self-assembly. Further, imidazole-based polymers readily associate with biological molecules through hydrogen-bonding.[25] Poly(*N*-vinyl imidazole) has been investigated as an agent to selectively bind metal ions in order to isolate them from wastewater. It was found that complexation occurred through the basic nitrogen atoms at position three of the imidazole ring.[30] Thus, we propose that a polymeric form of NAMI-A can also be synthesized using the reactive nitrogen on the imidazole ring.

Imidazole-containing polymers are typically obtained using free radical methods, which does not offer control of molecular weight and polymer architecture.[29] Dual stimuli-responsive block copolymers containing 1-vinylimidazolium monomers have been synthesized in a controlled manner using the RAFT/MADIX process,[31] and more recently Allen et al.[32] successfully polymerized 4-vinyl imidazole via RAFT, using a trithiocarbonate RAFT agent and glacial acetic acid as a distinctive solvent.

In this publication, we demonstrate for the first time that conjugation of NAMI-A to a nanoparticle can significantly enhance the drug performance, with respect to cytotoxicity and also the antimetastatic potential, creating an avenue for the better treatment of metastatic cancer. The aim of this work is to explore a synthetic avenue to a macromolecular version of NAMI-A, and also the synthesis of an amphiphilic block copolymer incorporating NAMI-A, that allows for the formation of micelles. 4-Vinyl imidazole was polymerized via RAFT and the formation of NAMI-A was examined. The NAMI-A micelles were then evaluated against different cancerous cell lines, and contrasted with the cytotoxicity of the NAMI-A drug alone. Finally, it was shown that the antimetastatic ability of NAMI-A was improved by incorporating it into a nanoparticle. The nanosized drug conjugate was significantly better at inhibiting the invasion of cells and also better at inhibiting the migration of cells, than NAMI-A alone.

■ EXPERIMENTAL SECTION

Chemicals. Urocanic acid (99%, Aldrich), 4,4′-azobis(cyanopentanoic acid) (ACPA; 98%, Fluka), glacial acetic acid (>99.5%, Aldrich), methanol (MeOH; HPLC grade, APS), ethanol (EtOH; absolute, Fluka), dimethyl sulfoxide (DMSO; >98.9%, Ajax Finechem), hydrochloric acid (HCl; 37%, Aldrich), acetone (HPLC grade, Aldrich), diethyl ether (99%, Ajax Finechem), imidazole (>95%, Fluka), ruthenium trichloride hydrate ($RuCl_3 \cdot H_2O$; Aldrich), poly(ethylene glycol) methyl ether acrylate (PEGMEA; Aldrich) were obtained as indicated. 2,2-Azobis(isobutyronitrile) (AIBN; 98%, Fluka) was purified by recrystallization from methanol. Milli-Q water was obtained from an UltraPure water purification system. The RAFT agent 2-(((dodecylthio)carbonothioyl)thio)-2-methylpropanoic acid was prepared according to a literature procedure.[33]

Analyses. *Size Exclusion Chromatography (SEC).* SEC was implemented using a Shimadzu modular system comprising a DGU-12A degasser, LC-10AT pump, SIL-10AD automatic injector, CTO-10A column oven, and a RID-10A refractive index detector. An Agilent aquagel−OH guard column and two linear columns (Agilent PL aquagel−OH Mixed-H and Mixed-M 8 μm particle size) were used for the analyses. A Milli-Q water/acetic acid/methanol (54:23:23) solution with a flow rate of 0.8 mL min^{-1} and a constant temperature of 30 °C was used as the mobile phase with an injection volume of 100 μL. The samples were filtered through 0.45 μm filters. The unit was calibrated using commercially available linear poly(ethylene oxide) standards (1900 − 909 500 g·mol^{-1}, Polymer Laboratories). Chromatograms were processed using Cirrus 2.0 software (Polymer Laboratories).

Nuclear Magnetic Resonance (NMR) Spectrometry. NMR general characterization was conducted using a Bruker Avance DPX 300 spectrometer (^{1}H, 300.2 MHz). Further characterization was conducted using a Bruker DMX 600 MHz spectrometer (^{1}H, 600.13 MHz) with a QNP probe and an Avance III 500 MHz spectrometer (^{1}H, 500.13 MHz) with a TBI probe. The 600 and 500 MHz spectrometer parameters are: 8390 Hz sweep width, 1.95 s acquisition time, 2 s recycle delay; 6009 Hz sweep width, 5.45 s acquisition time, 5 s recycle delay; respectively. The pulse program WATERGATE was used for water suppression.[34] Samples were analyzed in the solvents DMSO-d_6 and D_2O. All chemical shifts are stated in ppm (δ) relative to tetramethylsilane (δ = 0 ppm), referenced to the chemical shifts of residual solvent resonances (^{1}H and ^{13}C).

The solid-state NMR measurements were carried out on a Bruker Avance III 300 MHz spectrometer (^{1}H, 299.8 MHz). The samples were center packed in 4 mm zirconia rotors with Kel-F caps and spun up to 12 kHz in a Bruker 4 mm H-X double resonance wide bore solids probe head with variable temperature capability. The ^{1}H NMR T_{1H} measurements were done using a saturation recovery experiment involving a saturation comb made of 50 to a hundred delays of 30 μs to 1 ms duration each. The recycle delays were set to 100 ms with 256 to 512 transients detected for signal averaging.

X-ray Crystallography. Crystals were grown from a DCM/heptane layered solution in the glovebox. The single crystal of the compound for analysis was mounted on a Bruker APEXII CCD single crystal diffractometer equipped with graphite monochromated Mo K radiation.

Solid-State Elemental Analysis. Polymer samples were sent to The Campbell Microanalytical Laboratory at the University of Otago in New Zealand for elemental analysis.

Dynamic Light Scattering (DLS). Particle sizes were determined using a Brookhaven Zetaplus particle size analyzer (laser = 35 mW, λ = 632 nm, angle = 90°) and a solution of 1 mg mL^{-1} polymer in distilled water at 25 °C. Five measurements, with three runs consisting of 2 scans of 2 min in each measurement, were taken of each sample. Samples were purified from dust using a micro filter (0.45 μm) before analysis. The mean diameter was obtained from the arithmetic mean using the relative number or volume intensity of each particle size.

Transmission Electron Microscopy (TEM). The TEM micrographs were obtained using a JEOL1400 transmission electron microscope, consisting of a dispersive X-ray analyzer interfaced to the column and a Gatan CCD facilitating the acquisition of digital images. It was operated at an accelerating voltage of 80 kV. Samples were prepared by casting a 1 mg mL^{-1} polymeric micelle solution onto a copper grid. The grids were air-dried and then negatively stained with phosphotungstic acid for 2 min and air-dried again.

Thermo Gravimetric Analysis (TGA). Thermal decomposition properties of products were recorded using a TG5000 Thermogravimetric Analyzer. The sample (<1 mg) was placed on a thermo-balance

dx.doi.org/10.1021/ma402078d | *Macromolecules* XXXX, XXX, XXX−XXX

and heated from 25 to 1000 °C at 20 °C min^{-1} and held isothermally for 10 min under an air atmosphere.

UV−vis Spectrometry. Analyzed using a Varian Cary 300 UV−vis Spectrophotometer, fitted with a single cell chamber. Samples were analyzed at concentrations of 1−5 mg mL^{-1} in MeOH and water, from 200 to 800 nm at a scan rate of 600 nm min^{-1}.

Fourier-Transform Near-Infrared (FT-NIR) Spectroscopy. FT-NIR spectroscopy was used to determine monomer conversions by following the decrease of the vinylic stretching overtone of the monomer. A Bruker IFS 66\S Fourier transform spectrometer equipped with a tungsten halogen lamp, a CaF_2 beam splitter, and a liquid nitrogen cooled InSb detector was used. The sample was placed in a FT-NIR quartz cuvette (1 cm or 2 mm) and polymerized at 70 °C. Traces were elaborated with OPUS software.

Syntheses. *Synthesis of 4-Vinyl Imidazole (VIm).* 4-Vinyl imidazole (VIm) was synthesized following a modified literature procedure.[32] Urocanic acid (1.5 g, 1.1×10^{-2} mol) was heated to 240 °C under reduced pressure (2.2×10^{-2} mbar) for 6 h. The product distilled as a clear liquid, which solidified upon cooling to give 4-vinyl imidazole (4-VIm) as a waxy colorless solid (0.7 g, 66%). ^{1}H NMR (300.30 MHz, DMSO-d_6, 25 °C): δ (ppm) = 12.12 (s, 1H, NH), 7.61 (s, 1H, H_d); 7.06 (s, 1H, H_c); 6.57 (dd, 1H, H_b); 5.60 (dd, 1H, H_a); 4.99 (dd, 1H, H_a). ^{13}C NMR (300.30 MHz, DMSO-d_6, 25 °C): δ (ppm) = 136 (C_d); 135 (C_c); 128 (C_b); 120 (C_q); 110 (C_a).

Polymerization of 4-Vinyl Imidazole (PVIm) via RAFT Polymerization. VIm was polymerized following a literature procedure.[32] VIm (0.25 g, 2.7×10^{-3} mol), RAFT Agent (2-(((dodecylthio)-carbonothioyl)thio)-2-methylpropanoic acid) (5.0 mg, 1.3×10^{-5} mol) and ACPA (0.9 mg, 3.3×10^{-6} mol) as initiator, were dissolved in glacial acetic acid (3.3 mL) to give [VIm]:[RAFT]:[ACPA] = 200:1:0.25. The solution was transferred to a 10 mL Schlenk vial and deoxygenated by four freeze−pump−thaw cycles, and then placed in an oil bath at 70 °C. The polymerization was stopped after 24 h by cooling the vial and opening to air. The solution was dialyzed (MWCO = 3500 g mol^{-1}) against Milli-Q water and dried under vacuum to give poly(4-vinyl imidazole) (PVIm) as a pale yellow low density solid (0.16 g). Total reaction time = 24 h, x_{NMR} = 76%, x_{Mass} = 65%, $M_{n,theo}$ = 14 300 g mol^{-1}. ^{1}H NMR (300.30 MHz, MeOD, 25 °C): δ (ppm) = 7.52 (broad, 1H, H_d); 6.35 (broad, 1H, H_c); 2.40−1.90 (broad, 1H, H_b); 1.62 (broad, 2H, H_a).

Chain Extension of 4-Vinyl Imidazole with Poly(ethylene glycol) Methyl Ether Acrylate (PVIm-PPEGMEA) via RAFT Polymerization. PEGMEA (0.1 g, 2.3×10^{-4} mol), VIm MacroRAFT (40 mg, 4.6×10^{-6} mol), and AIBN (0.2 mg, 9.3×10^{-7} mol) as initiator, were dissolved in MeOH (0.45 mL) to give [PEGMEA]:[PVIm]:[AIBN] = 50:1:0.2. The solution was transferred to a 10 mL Schlenk vial and deoxygenated by five freeze−pump−thaw cycles. The solution was subsequently transferred to a 2 mm FT-IR quartz cuvette in a glovebox, and placed in the preheated FT-IR cell at 65 °C. The polymerization was monitored over time and stopped after 4 h by cooling the cuvette and opening to air. The solution was dialyzed (MWCO = 3500 g mol^{-1}) against Milli-Q water and dried under vacuum to give poly(4-vinyl imidazole)-*b*-poly(poly(ethylene glycol) methyl ether acrylate) (PVIm-PEGMEA) as a pale yellow rubbery solid (96 mg). Total reaction time = 4 h, $x_{FT\text{-}NIR}$ = 48%, x_{Mass} = 63%, $M_{n,theo}$ = 28 700 g mol^{-1}. ^{1}H NMR (300.30 MHz, MeOD, 25 °C): δ (ppm) = 7.54 (broad, 1H, H_d); 6.42 (broad, 1H, H_c); 4.23 (broad, 2H, H_g), 3.63 (broad, PEG), 3.53 (broad, 2H, H_h), 3.32 (broad, 3H, H_1), 2.79 (broad, 1H, H_f), 2.40−1.90 (broad, 1H, H_b); 1.60 (broad, 4H, H_a and H_e).

Synthesis of [$DMSO_2H$][trans-$RuCl_4(DMSO)_2$] (Ru Precursor). [$DMSO_2H$][*trans*-$RuCl_4(DMSO)_2$] (Ru precursor) was synthesized following a literature protocol.[35,36] Ruthenium trichloride hydrate ($RuCl_3.H_2O$) (1.5 g, 7×10^{-3} mol) was combined with dimethyl sulfoxide (DMSO) (7.0 mL) in a 100 mL round-bottom flask. Hydrochloric acid (HCl) (32%) (1.2 mL) was added and the solution heated to 80 °C for 20 min with vigorous stirring. The solution turned a deep red color and the temperature was increased to 100 °C and kept at this temperature for 20 min, at which time the solution was an orange-red color. The solution was cooled to room temperature with stirring, and acetone (50 mL) and diethyl ether (5 mL) were added. The solution was transferred into a conical flask and placed in a dark cupboard to allow for crystal formation. Large red-orange crystals were washed with diethyl ether, dried under vacuum, and confirmed by X-ray crystallography to be consistent with literature.[36] ^{1}H NMR (600.13 MHz, D_2O, 25 °C): δ (ppm) = 2.74 (s, 6H, [$DMSO_2H$]); −16.62 (very broad, 6H, [*trans*-$RuCl_4(DMSO)_2$]).

Synthesis of (ImH)[$Ru^{III}Cl_4$(Im)(S-DMSO)] (NAMI-A). (ImH)-[$Ru^{III}Cl_4$(Im)(*S*-DMSO)] (NAMI-A) was synthesized following a literature procedure.[37] [$DMSO_2H$][*trans*-$RuCl_4(DMSO)_2$] (0.1 g, 1.8×10^{-4} mol) was crushed to a mustard-yellow powder and suspended in acetone (2.0 mL) with stirring. Imidazole (50 mg, 7.4×10^{-4} mol) was then slowly added while rapidly stirring. The reaction was left rapidly stirring for 4 h, after which time the product was filtered, washed with acetone (3.0 mL) and diethyl ether (3.0 mL), and dried under vacuum, to give a mustard yellow-orange solid (54 mg, 65%). The compound was confirmed by ^{1}H NMR to be consistent with literature. ^{1}H NMR (600.13 MHz, D_2O, 25 °C): δ (ppm) = 8.71 (s, 1H, ImH); 7.50 (s, 1H, ImH); −3.43 (broad, 1H, Im); −5.13(broad, 1H, Im); −6.54(broad, 1H, Im); −15.1 (very broad, 6H, (*S*-DMSO).

Synthesis of Macromolecular NAMI-A [P(NAMI-A)]. In a typical preparation, [$DMSO_2H$][*trans*-$RuCl_4(DMSO)_2$ (15 mg, 2.7×10^{-5} mol) was crushed to an orange powder and dissolved in ethanol or methanol (1 mL). PVIm (10 mg, 1.1×10^{-4} mol) was suspended in the same solvent (1 mL). The solutions were combined and stirred to give a mustard yellow suspension. For cytotoxicity assays, the solution was diluted with water and used immediately. For UV−vis analysis, the solution was diluted with methanol. For elemental, NMR, and TGA analyses, the product was filtered, washed with diethyl ether (2 mL), and dried under vacuum, to give a mustard brown solid.

Synthesis of Amphiphilic Block Copolymer P(NAMI-A)-PPEGMEA. In a typical preparation, [$DMSO_2H$][*trans*-$RuCl_4(DMSO)_2$ (4.6 mg, 7.9×10^{-6} mol) was crushed to an orange powder and dissolved in methanol (1 mL). PVIm-PPEGMEA (5.1 mg, 3.2×10^{-5} mol) was also dissolved in MeOH (1 mL). The solutions were combined to give a bright yellow solution and analyzed via UV−vis immediately. For cytotoxicity assays, the solution was slowly diluted (1 h) and then dialyzed against MQ water for 1 h and used immediately. For solid-state NMR, the solution was vacuum-dried to give an orange solid.

In Vitro Cytotoxicity Assay. Human ovarian carcinoma A2780 and Ovcar-3, and pancreatic AsPC-1 cells were cultured in 75 cm^2 tissue culture flasks with RPMI 1640 medium supplemented with 10% fetal bovine serum, 4 mM glutamine, 100 U/mL penicillin, 100 μg mL^{-1} streptomycin, and 1 mM sodium pyruvate at 37 °C under an atmosphere of 5% CO_2. After reaching 70% confluence, the cells were washed with phosphate buffered saline (PBS) and collected by trypsin/EDTA treatment. The cells were seeded in 96-well cell culture plates at 4000 cells per well and cultured at 37 °C for one day. The medium in the cell culture plate was discarded and 100 μL fresh 2 × concentrated RPMI 1640 serum medium was added. The samples were added into the plate at 100 μL per well for 72 h. Before loading onto the cells, solutions were sterilized by UV irradiation for 15 min in a biosafety cabinet and then serially diluted (2 × dilution) with sterile water and incubated for 2 h at room temperature. The working concentration of ethanol in the culture medium was adjusted to 1 v/v % in case of PVIm and P(NAMI-A) samples. One v/v % ethanol did not show significant influence on the viability of A2780, Ovcar-3 and AsPC-1 cells.

The cell viability was measured using a WST-1 assay (Roche Diagnostics). This is a colorimetric assay for the quantification of cell viability and proliferation that is based on the cleavage of a tetrazolium salt (WST-1) by mitochondrial dehydrogenases in viable cells. Increased enzyme activity leads to an increase in the amount of formazan dye, which is measured with a microplate reader. After incubation for three days, the culture medium was removed and 100 μL fresh medium was added along with 10 μL WST-1. The plates were then incubated for an additional 4 h at 37 °C. After incubation, the absorbance of the samples against the background control on a Benchmark Microplate Reader (Bio-Rad) was obtained at a wavelength of 440 nm with a reference wavelength of 650 nm. Four wells

dx.doi.org/10.1021/ma402078d | *Macromolecules* XXXX, XXX, XXX−XXX

under each condition were used for the measurement to calculate the means and standard deviations. All cytotoxicity data are reported as mean ± standard deviation. A two-tailed student's *t* test was executed to reveal the statistical differences. A p-value less than 0.05 was considered statistically significant.

Antimetastatic Assay. The highly invasive MDA-MB-231 human breast cancer cell line was obtained from the Australia Cell Bank. The MCF-7 human breast cancer cell line was kindly supplied by the Lowy Cancer Research Centre (UNSW, Sydney, Australia). The non-tumorigenic Chinese hamster ovary (CHO) cells were kindly supplied by St. George Hospital. The three cell lines were cultured in 75 cm^2 tissue culture flasks with a complete medium composed of Dulbecco's Modified Eagle Medium (DMEM) supplemented with 10% FBS, 4 mM glutamine, 100 U mL^{-1} penicillin, 100 $\mu g \cdot mL^{-1}$ streptomycin, 1 mM sodium pyruvate and 1% MEM nonessential amino acid at 37 °C under an atmosphere of 5% CO_2. After reaching 70% confluence, the cells were washed with PBS and collected by trypsin/EDTA treatment. The cells were seeded in 6-well cell culture plates and incubated for 1 day before P(NAMI-A)-PPEGMEA, NAMI-A, and PVIm-PPEGMEA treatment. The Ru concentration in P(NAMI-A)-PPEGMEA and NAM-A was 5 μM. The polymer concentrations in both P(NAMI-A)-PPEGMEA and PVIm-PPEGMEA was 3.5 $\mu g \cdot mL^{-1}$.

Chemotaxis and Haptotaxis. The migratory ability resulting from a haptotactic or a chemotactic stimulus was measured in 24-well Millicell hanging cell culture inserts (Millipore, Billerica, MA) by the methods of Bergamo et al. with some modifications.[38] In the haptotaxis assay the lower surface of a polyethylene terephthalate (PET) filter (8-μm pore size) was coated with 10 $\mu g \cdot mL^{-1}$ fibronectin and left in a humidified cell culture chamber at 4 °C overnight, then washed with PBS before cell seeding. In the chemotaxis assay, inserts were used without coating. Cells were treated for 1 h with all the samples in the complete medium. Then the cells were washed with PBS three times, collected by trypsinisation and centrifugation, and resuspended in serum-free medium supplemented with 0.1% w/v bovine serum albumin (BSA). A 0.2 mL cell suspension at 5×10^5 cells$\cdot mL^{-1}$ was seeded in the upper compartment of each insert. The lower compartment was filled with serum free medium supplemented with 0.1% w/v BSA and with complete medium for the haptotaxis and the chemotaxis assay, respectively. Cells were incubated at 37 °C for 24 h, and then the cells on the upper surface of the filters were removed with a cotton swab. The migrated cells in the lower surface were washed with PBS, trypsinized with 0.3 mL of trypsin/EDTA, and counted by a hemacytometer.

Invasion Assay. 24-well Millicell hanging cell culture inserts (8-μm pore size) were coated with 50 μL of 1 mg.mL^{-1} Matrigel (diluted in serum-free DMEM medium; BD Sciences, Franklin Lakes, NJ) and air-dried overnight at room temperature. The filters were reconstituted with serum free medium immediately before use. Then, 2.5×10^5 cells in 0.2 mL of serum free medium (with 0.1% BSA) were added to the upper chamber and the lower compartment was filled with complete medium. The cells were allowed to invade for 48 h at 37 °C in a CO_2 incubator. Then the cells on the upper surface of the filters were removed with a cotton swab. The invading cells on the lower surface were washed with PBS, trypsinized with 0.3 mL trypsin/EDTA and counted by a hemacytometer.

Cell Viability Assay. The effects on the cell viability of P(NAMI-A)-PPEGMEA, NAMI-A and PVIm-PPEGMEA were evaluated by a WST-1 assay. The cells were seeded on 96-well plates at 4 000 cells/well and incubated for 24 h. The samples were loaded to the cell with the complete medium and cultured for 72 h at 37 °C in the incubator. The viability was measured by the WST-1 assay as described above.

Cells without sample treatment were used as controls. Each assay was done in triplicate. Data represent means ± SD. A one way analysis of variance was used to reveal the statistical difference among different groups. A Dunnett's post hoc test was used to compare the difference between samples and the control. A *p*-value less than 0.05 was considered a statistically significant difference.

RESULTS AND DISCUSSION

Synthesis and Polymerization of 4-Vinyl Imidazole. Consistent with the observations by Allen et al.[32] we were unable to synthesize the water-soluble[28] poly(*N*-vinyl imidazole) in a controlled manner by RAFT polymerization since it forms a highly reactive and unstable propagating radical due to the absence of resonance stabilization. In contrast, 4-vinyl imidazole (VIm) could be polymerized via RAFT, using the trithiocarbonate RAFT Agent (2-(((dodecylthio)-carbonothioyl)thio)-2-methylpropanoic acid) and glacial acetic acid as a distinctive solvent, due to the increased radical stability. VIm was synthesized and subsequently polymerized (Scheme S1, Supporting Information) following a modified literature procedure.[32] Urocanic acid was heated under reduced pressure to decarboxylate and distill as a clear liquid, which solidified upon cooling to give a waxy colorless solid. The product was confirmed by ^{1}H NMR spectroscopy (Figure S1).

The monomer was subsequently polymerized via RAFT polymerization (Scheme 1 and Figure S2, Supporting Information) to give a colorless solid that was soluble in methanol, DMSO and a water/ethanol mixture. The polymerization was monitored using water-based SEC (Figure S3, Supporting Information) and shown to be consistent with previous observations by Allen et al.[32] as the molecular weight, shown by the change in retention time, of the polymer increased over time.

The $[DMSO_2H][trans\text{-}Ru^{III}Cl_4(DMSO)_2]$ (Ru Precursor) complex (Scheme 1 and Scheme S2, Supporting Information)

Scheme 1. Synthesis of the Amphiphilic Block Copolymer P(NAMI-A)-PPEGMEA Using 2-(((Dodecylthio)carbonothioyl)thio)-2-methylpropanoic Acid RAFT Agent and Micellization in Water

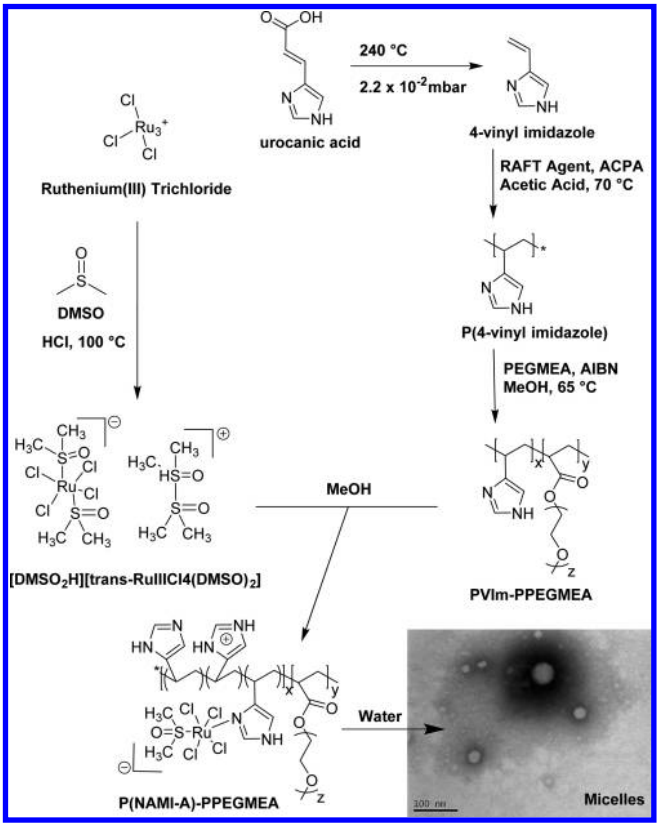

dx.doi.org/10.1021/ma402078d | *Macromolecules* XXXX, XXX, XXX–XXX

that is used in the synthesis of the antimetastatic coordination compound NAMI-A was synthesized following a literature procedure[35,36] and confirmed by X-ray crystallography to be consistent with literature (Table S1, Supporting Information).[36]

Because of the unfavorable occurrence of two trans *S*-bonded DMSO's in the precursor complex, substitution of at least one of them with a stronger σ-donor ligand is a relatively simple task.[36] Alessio et al.[35] reported that one DMSO ligand can rapidly be replaced in an organic solvent at room temperature using a slight excess of a nitrogen ligand. Hence, NAMI-A (Scheme 2) was synthesized following a literature procedure,[37]

Scheme 2. Synthesis of (ImH)[$Ru^{III}Cl_4$(Im)(*S*-DMSO)] (NAMI-A) and M-NAMI-A in Acetone at Room Temperature[a]

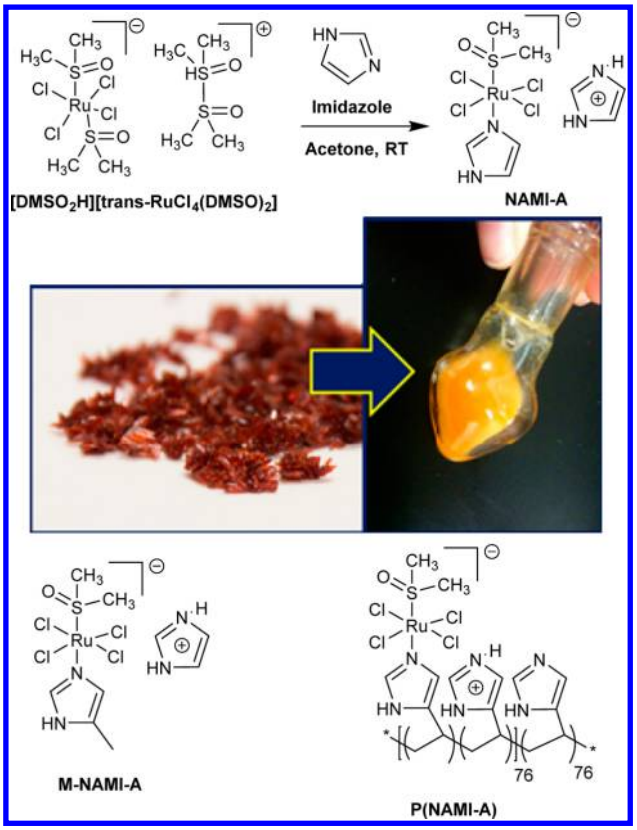

[a]P(NAMI-A) was prepared in ethanol. The photos depict the orange colored crystals of the precursor and the mustard-yellow-colored product.

using an excess of imidazole, and characterized via ^{1}H NMR spectroscopy (Figure S4) and confirmed to be consistent with literature due to the very broad DMSO methyl peak at −15.2 ppm.

A polymeric form of NAMI-A [P(NAMI-A)] was synthesized by combining PVIm ($M_{n,theo}$ = 14 300 g·mol^{-1}) and the Ru Precursor in ethanol or methanol. A methylated version of NAMI-A (using 4-methyl imidazole) was also synthesized as a control for comparison, since the homopolymer was synthesized from 4-vinyl imidazole. Following a literature procedure for the synthesis of NAMI-A,[37] the imidazole was added in a 4:1 excess to the Ru precursor, to ensure complete conjugation of ruthenium to imidazole, and the formation of imidazole counterions (previous research has shown that the imidazole counterion imparts more favorable chemical properties on NAMI-A than other counterions, for example Na^+).[5]

Consistent with the synthesis of NAMI-A, the Ru precursor was first dissolved in the selected solvent (methanol for P(NAMI-A) and acetone for M-NAMI-A) giving a bright orange solution. The imidazole (PVIm or 4-methyl imidazole) was subsequently added while vigorously stirring, immediately producing a yellow-orange suspended precipitate. The solid was washed to remove any unreacted materials and dried under vacuum. The UV−vis absorbance maxima of the products in methanol were compared (Figure 1). A clear shift from the Ru

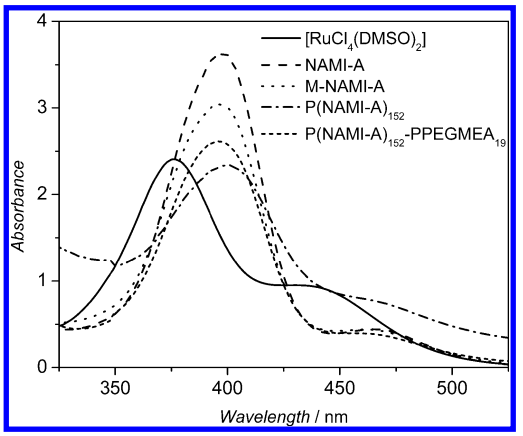

Figure 1. UV−vis spectrum in methanol at 25 °C. The attachment of imidazole to Ru^{III} elicits a clear shift in absorbance maxima from 375 to 400 nm.

precursor at 375 nm to NAMI-A, M-NAMI-A and P(NAMI-A) at 400 nm, indicated complete substitution of one DMSO ligand with an imidazole, producing the desired products.

Thermogravimetric analysis was used to confirm the amount of ruthenium in each sample (Table 1). A dry polymer sample

Table 1. Thermogravimetric Analysis of NAMI-A Analogues[a]

sample	Ru precursor[c]	NAMI-A	M-NAMI-A	P(NAMI-A)
residue (%) using N_2	21	23	21	13
residue (%) using O_2	24	29	23	21
Ru (%)[b]	18	22	17	16
Ru (% theo)[d]	18.16	22.11	20.83	–

[a]Samples were analyzed using both nitrogen and oxygen to degrade the samples. [b]Ru fraction = (mass residue using O_2 × 0.759)/initial mass. [c]Ru precursor = [$DMSO_2H$][*trans*-$RuCl_4$(DMSO)$_2$]. [d]Calculated from the structural formula.

was loaded onto a TGA pan and heated to 1000 °C at a rate of 20 °C·min^{-1}. Since ruthenium oxidizes to RuO_2 at 600 °C, 75.9% of the residual mass can be ascribed to ruthenium, assuming that the residue is pure RuO_2.

In addition, a dry P(NAMI-A) polymer sample was submitted for solid-state elemental analysis. The number of imidazole repeating units was calculated from the NMR conversion (n = 152). A spread sheet was then constructed to determine the number of imidazole units that had ruthenium attached, thus forming NAMI-A, assuming that for each imidazole with ruthenium there is another imidazole that acts as a counterion. It was found that 49% of the polymer units were NAMI-A units (Table S2, Supporting Information). This

dx.doi.org/10.1021/ma402078d | *Macromolecules* XXXX, XXX, XXX−XXX

is consistent with the complete conjugation (within error) of all added ruthenium since the Ru precursor was combined with a 4:1 excess of imidazole units and two imidazole units form NAMI-A (one conjugated to ruthenium and the other forming the positively charged counterion). The fraction of ruthenium calculated from TGA is also consistent with the calculated percentage. The remaining error is due to the nature of polymer entities and the variability between polymer chains. The resulting structure with the calculated repeating unit is depicted in Scheme 2.

The P(NAMI-A) polymer is barely soluble in any solvent (including water). This low solubility in water is advantageous as it provides an avenue to the formation of nanoparticles. One of the primary motivations for incorporating anticancer drugs into polymers is to increase cell uptake in the body. Since P(NAMI-A) is insoluble in water, it can act as the hydrophobic component of polymeric micelles, which have been shown to have better cell uptake than linear polymers.[39] Therefore, a suitable comonomer, namely poly(ethylene glycol) methyl ether acrylate (PEGMEA), was chosen and PVIm was used as a macroRAFT agent and chain extended with PEGMEA (Figure S5). The monomodal SEC trace (Figure 2) shows a clear shift

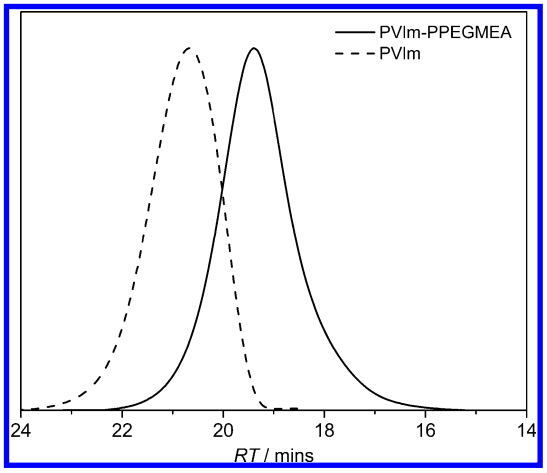

Figure 2. Water SEC trace of the polymerization of poly(ethylene glycol) methyl ether acrylate in methanol at 65 °C using P(4-vinyl imidazole) MacroRAFT agent ($M_{n,theo}$ = 14 300 g mol^{-1}). [PEGMEA] = 0.4 M, [PEGMEA]:[PVIm]:[AIBN] = 50:1:0.2. Total reaction time = 4 h, $x_{FT\text{-}NIR}$ = 48%, $M_{n,theo}$ = 28 700 g mol^{-1}. The eluent was a Milli-Q water/acetic acid/methanol (54:23:23) solution.

in retention time, indicative of a molecular weight change and a successful chain extension. The absence of any low molecular weight shoulder indicates that the PVIm MacroRAFT is quite efficient in mediating the polymerization of PEGMEA. Since the M_n values obtained from the water SEC traces cannot be used due to the difference in the polymer and the PEO calibration standards, the molecular weights used in further discussions were calculated using conversions determined from FT-NIR.

The Ru precursor was reacted with the copolymer P(NAMI-A)$_{152}$-PPEGMEA$_{19}$ in a similar fashion to the homopolymer – the difference being that the copolymer remained soluble in methanol after conjugation, and it could be dried and redissolved. Because of the difference in solubilities, the homopolymeric drug was purified by washing with methanol, whereas the copolymeric drug was purified by dialysis. UV–vis was used to confirm the complexation. Figure 1 shows a shift in the UV–vis absorbance maxima for P(NAMI-A)-PPEGMEA, comparable to that of NAMI-A and P(NAMI-A).

Solution NMR was used as a final analysis method to confirm the complex formation of NAMI-A. However, this was not possible for the macromolecular forms of NAMI-A – neither homopolymer nor copolymer. Paramagnetism of the Ru^{III} nucleus combined with the inherent broadening of polymer signals prevented a detailed solution NMR study. Solid-state NMR was thus used to determine the homogeneity of NAMI-A within the P(NAMI-A) and P(NAMI-A)-PPEGMEA polymers.

The presence of paramagnetic Ru^{III} causes fast relaxation with concomitant line broadening and paramagnetic contact shift in the ^{1}H and ^{13}C solid state NMR of these materials. As a result using chemical shift to measure incorporation and bonding of the Ru^{III} species is challenging. An alternative method is to look at the spin–lattice relaxations of the ^{1}H (T_{1H}) where the presence of a paramagnetic species would cause enhanced relaxation of the ^{1}H nuclei. The T_{1H} was measured by a saturation recovery experiment where the equilibrium magnetization was first suppressed by a comb of saturation pulses and delays after which a recovery delay was introduced for the ^{1}H magnetization to recover. The total integrated area of the ^{1}H NMR signal (normalized against M_0, the signal area for the fully recovered magnetization) was plotted against the recovery time (ms) as seen in Figure 3. The

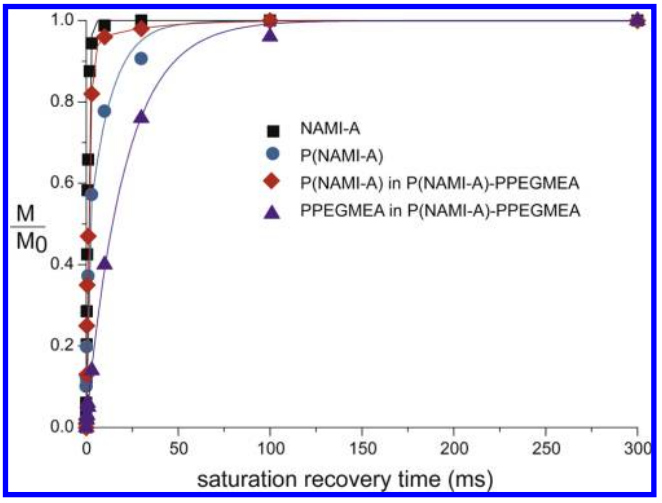

Figure 3. ^{1}H saturation recovery experiment of NAMI-A, P(NAMI-A), and P(NAMI-A)-PPEGMEA via solid-state NMR.

data was fitted by a single or double exponential of the form $M/M_0 = 1 - A\exp^{-t/T_{1A}} - B\exp^{-t/T_{1B}}$, where A and B are the fractions of slow and fast relaxing components with spin–lattice relaxation times of T_{1A} and T_{1B}. It should be noted that in the case of paramagnetic driven relaxation processes, the saturation recovery behavior can be nonexponential (stretched exponential) particularly in the case of low natural abundance NMR active nuclei such as ^{13}C.[40] However in the case of nuclei such as ^{1}H in the current materials with fast nuclear spin diffusion and moderate MAS (12 kHz), the saturation recovery behavior is better described by a single or double exponential curve.

For example, the ^{1}H saturation recovery of the neat NAMI-A complex is well fitted by a single exponential with a T_{1H} of 0.9 ms. The extremely fast T_{1H} is consistent with the presence of the paramagnetic Ru^{III} in the solid material. In the case of the P(NAMI-A), the overall fast spin–lattice relaxation of the ^{1}H species, confirmed the attachment of a paramagnetic species,

dx.doi.org/10.1021/ma402078d | Macromolecules XXXX, XXX, XXX–XXX

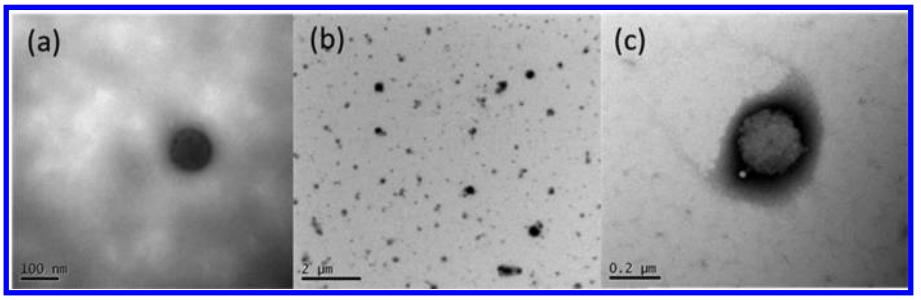

Figure 4. P(NAMI-A)-PPEGMEA Micelles were prepared by dialyzing a MeOH solution against water, and analyzed by TEM and DLS. Sample a was drop-loaded onto a grid and air-dried. Samples b and c were drop-loaded onto the grid, air-dried, and stained with phosphotungstic acid. Scale bar: a = 100 nm; b = 2 μm; c = 0.2 μm;.

and thus it can be inferred that ruthenium is still present as Ru^{III}. However the saturation recovery curve P(NAMI-A) followed a dual exponential behavior. The faster relaxing component with a very fast T_{1H} relaxation time of 0.5 ms corresponded to 45% of the polymer that is at an average distance of ca. 1 nm from the Ru^{III} complex, while the comparatively slower T_{1H} relaxation time of 12 ms corresponded to ca. 55% of the polymer beyond nanometer proximity of the Ru^{III} complex. This is consistent with the elemental analysis and TGA results, which showed that approximately 50% of the imidazole units formed NAMI-A.

Finally, the absence of any slow relaxing components with a T_{1H} in the order of 100 ms to several seconds, as would be expected for diamagnetic, amorphous, organic polymers, implies that on a conservative 10 nm scale there is a uniform distribution of the Ru^{III} complex within the P(NAMI-A) polymer matrix.

In the case of the P(NAMI-A)-PPEGMEA the ^1H spectrum of the copolymer yields two peaks—one broad and one narrow. The broad component corresponds to the rigid P(NAMI-A) block containing the Ru^{III} complex with a fast T_{1H} of ca. 1.5 ms relaxation. The narrow component corresponds to the mobile PPEGMEA block which, as expected, has a distinctly longer relaxation time (28 ms) than the P(NAMI-A) block. It is likely that the PPEGMEA block is strongly coupled to the faster-relaxing proton pool of the P(NAMI-A) block accounting for a T_{1H} of ca. 28 ms. It is highly unlikely that the PPEGMEA contains Ru^{III} since there are no binding sites in this copolymer block to allow for the formation of the ruthenium complex. Additionally, the UV−vis spectrum (Figure 1) confirmed the attachment of the Ru^{III} complex to the imidazole units in the PVIm block, as shown by a clean shift of a single peak, and there was no indication of Ru^{III} interacting with the PPEGMEA block in the polymer. However, approximately 6% of the P(NAMI-A) block has a longer relaxation time of ca. 20 ms. We hypothesize that this can be attributed to the region where both blocks are connected and that the proximity to the PEG induces motional mobility to a fraction of the P(NAMI-A) which can enhance the relaxation times. Considering the relatively small fraction of the P(NAMI-A) block with the longer relaxation time, it is also possible that it has a lower Ru^{III} concentration. However, given the synthesis method, it is unlikely that the Ru^{III} would distribute heterogeneously within the PVIm copolymer block, since it is homogeneous in the homopolymer on the 10 nm scale. Overall, these results are consistent with the distinct PPEGMEA and P(NAMI-A) phases, where the predominant fraction of the PPEGMEA phase is further from the paramagnetic centers.

In summary, these results clearly suggest the following:

(a) The overall fast relaxation indicates that the complex is incorporated into the polymer.
(b) The comparatively longer relaxation time (12 ms) indicates that on the 10 nm scale, there is homogeneous distribution of the complex.
(c) The short relaxation time (0.5 ms) corresponds to the region within nanometer scale proximity of the complex. It also indicates that the complex is dispersed within the polymer and has not aggregated.
(d) The copolymer ^1H spectrum consists of a broad and narrow component with very different relaxation properties, indicative that Ru^{III} is incorporated uniformly in a single block of the polymer, i.e., P(NAMI-A).

After drug conjugation, the methanol solution was immediately dialyzed against water to remove methanol and simultaneously form micelles in solution. The dialyzed yellow solutions were analyzed using TEM and DLS (Figure 4 and 5)

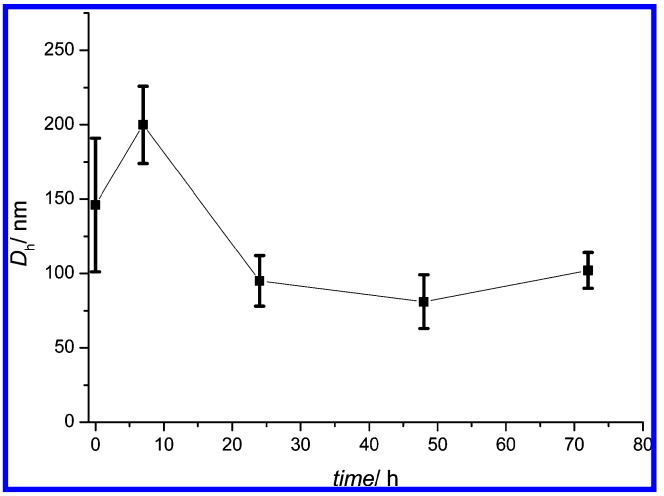

Figure 5. Stability of micelles as determined by DLS (volume distribution) in phosphate buffered saline (pH 7.4) at 37 °C over 3 days.

to determine micelle size and homogeneity. TEM shows micelles to be a reasonable size, although a size distribution is evident. This distribution was also apparent in the DLS measurements, indicated by the PDI. The micelles are round in shape, but probably slightly distorted due to the drying process for TEM preparation. The unstained sample in Figure 4a appears black due to the conjugation of ruthenium, which has a high electron density. Closer inspection of Figure 4a reveals the darker appearance of the center of the micelle due to the location of ruthenium in the core of the micelle.

dx.doi.org/10.1021/ma402078d | *Macromolecules* XXXX, XXX, XXX−XXX

The size of the micelle in PBS buffer was in addition confirmed using DLS (Figure 5). Directly after dialysis of the methanol solution against aqueous solution the size distribution was found to be broad as indicated by the large error bars. After an intermittent size increase, probably due to aggregate formation, the micelle size was stable over several days with an average hydrodynamic volume of approximately 90 nm with a low distribution. However, the degradation of the drug during that long period of time cannot be avoided and color changes are visible.

***In Vitro* Cytotoxicity and Antimetastatic Potential.** The NAMI-A polymeric micelles were tested against ovarian A2780 and Ovcar-3 and pancreatic AsPC-1 cancer cell lines, and compared with the drug NAMI-A. The homopolymer and block copolymer prior to drug conjugation were also tested for toxicity (Table 2, Figure 6). PVIm was found to be toxic, which

Table 2. IC_{50} Values with Respect to the Polymer Concentration, against Ovarian A2780 and Ovcar-3 and Pancreatic AsPC-1 Cancer Cell Lines

	IC_{50} ([P], μM)		
	A2780	AsPC-1	OVCAR-3
PVIm	0.37	0.51	0.70
PVIm-PPEGMEA	>15.37	>15.37	>15.37
P(NAMI-A)-PPEGMEA[a]	9.77	8.86	9.65

[a]Polymer concentrations at IC_{50} in Table 3.

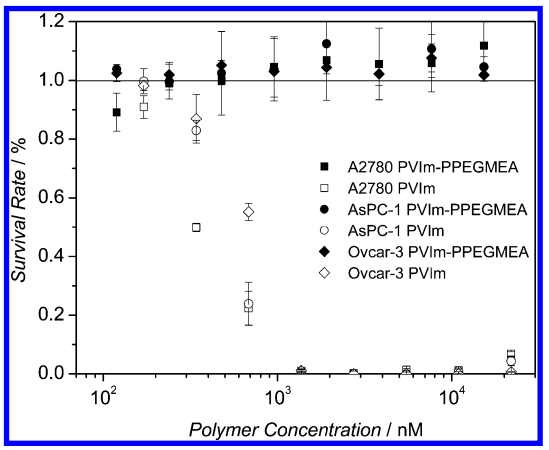

Figure 6. Cytotoxicity of PVIm and PVIm-PPEGMEA against ovarian A2780 and Ovcar-3 and pancreatic AsPC-1 cancer cell lines.

makes P(NAMI-A) an undesirable therapeutic agent, since the toxicity is derived from the polymer itself and not the drug. This can be attributed to the positive charges of the imidazole units, as positively charged polymers have previously shown toxicity.[41] The copolymer, PVIm-PPEGMEA, was completely nontoxic to all cell lines up to a concentration of 10 μM. This was surprising since the copolymer still contains unmodified PVIm. The reason for this complete lack of toxicity can be attributed to the morphology of the block copolymer, since the homopolymer PVIm is insoluble in water. This may lead to the micelle formation of PVIm-PPEGMEA, with positively charged PVIm forming the core of the micelle. The sudden disappearance of apparent cytotoxicity has been observed earlier when a cationic polymer formed the core of a cross-linked micelle resulting in the loss of toxicity in this assay.[42]

A statistically significant decrease in the IC_{50} values for P(NAMI-A)-PPEGMEA micelles compared with NAMI-A alone at the same ruthenium concentration, was found for all cell lines (Table 3, Figure 7). The micelles were found to be

Table 3. IC_{50} Values with Respect to the Ruthenium Concentration, against Ovarian A2780 and Ovcar-3 and Pancreatic AsPC-1 Cancer Cell Lines

	IC_{50} ([Ru], μM)		
	A2780	AsPC-1	OVCAR-3
NAMI-A literature	>500[43]	–	–
NAMI-A	595.6 ± 28.5	601.7 ± 13.5	737.8 ± 38.0
P(NAMI-A)-PPEGMEA	438.7 ± 14.8	397.6 ± 24.7	433.4 ± 26.8

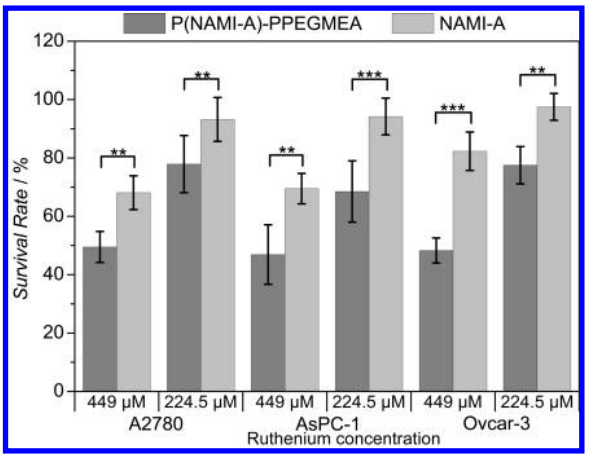

Figure 7. Cytotoxicity of NAMI-A and P(NAMI-A)-PPEGMEA against ovarian A2780 and Ovcar-3 and pancreatic AsPC-1 cancer cell lines. For P(NAMI-A)-PPEGMEA, the polymer concentration at [Ru] = 449 and 224.5 μM is 10 and 5.0 μM respectively. Mean ± SD, n = 4, (**) significantly different p < 0.01, (***) significantly different p < 0.001.

~1.5 times better than NAMI-A at inhibiting cancer cell growth, across the tested cell lines. Most notably, they were active on the highly aggressive pancreatic cancer cell line. However, IC_{50} values cannot be solely relied upon to determine the efficacy of a particular drug, since there are many determining factors for a drug to enter into clinical trials, for example the drug's ability to reach the target.

It has previously been established by Sava and co-workers that, for NAMI-A-type compounds, *in vitro* inhibition of tumor invasion correlates with the *in vivo* inhibition of metastasis formation.[44−46] Bergamo et al.[38] subsequently developed a series of experiments that simulate *in vitro* the main steps of metastatic progression: detachment from the primary tumor, degradation of the extracellular matrix, ability to migrate, invade and adhere to a new organ. These protocols were adapted to assess the antimetastatic potential of P(NAMI-A)-PPEGMEA micelles compared with NAMI-A.

The migration and invasion assays were chosen to assess the antimetastatic potential of the ruthenium conjugated P(NAMI-A)-PPEGMEA micelles in comparison to the antimetastatic drug NAMI-A. The effects of NAMI-A, the block copolymer without ruthenium, and the micelles incorporating NAMI-A were evaluated against three cell lines characterized by differing degrees of malignancy (MDA-MB-231 > MCF-7 > CHO).

dx.doi.org/10.1021/ma402078d | *Macromolecules* XXXX, XXX, XXX−XXX

A ruthenium concentration of 5 μM was chosen as a suitable concentration to be used for the following experiments since the cell viability was unaffected by the compounds at this concentration. Higher ruthenium concentrations would lead to significant cell deaths and the measurement of the migration would therefore be inaccurate. Figure S6 (Supporting Information) shows that the ruthenium compound induces only slight and nonsignificant oscillations (±10%) in cell viability as compared to the relevant controls. This is necessary in order to exclude the interference of the cytotoxicity of the compounds in the following assays.

The influence of the compounds on the migration process of the three cell lines MDA-MB-231 (invasive cancerous), MCF-7 (noninvasive, cancerous) and CHO (noncancerous) was evaluated when a chemical (chemotaxis) and a contact (haptotaxis) stimulus was applied to promote cell movement (Figure 8 and Figure 9). The chemotactic and haptotactic

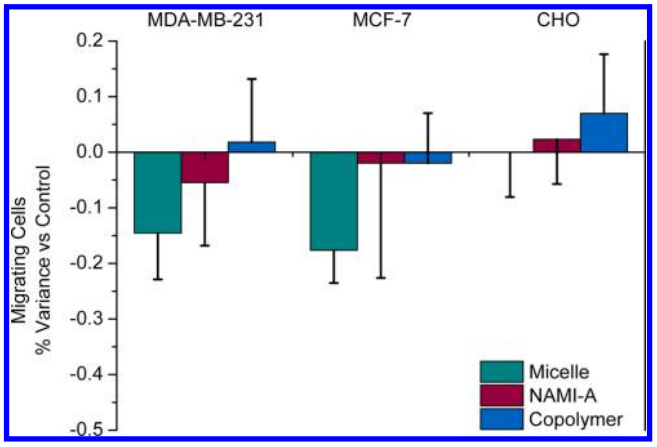

Figure 8. Effect of NAMI-A, PVIm-PPEGMEA, and P(NAMI-A)-PPEGMEA Micelles on the chemotactic migration of cells through polycarbonate filters. MDA-MB-231, MCF-7 and CHO cell were treated for 1 h with the drugs where [Ru] = 5 μM. The cells were then removed from the flasks, collected, resuspended and seeded on the insets of Transwell cell culture chambers. Data represent cells that after 24 h have migrated and are present on the lower surface of the filter. Data are the percent of variation vs controls calculated from the mean ± SD of one experiment performed in triplicate.

migration of both the MDA-MB-231 and MCF-7 cells was inhibited more than that of the CHO cells. However, no statistically significant effect was observed with respect to the controls.

The effect on the invasive ability of these cells through Matrigel was also assessed (Figure 10). The invasive ability of both the MDA-MB-231 and MCF-7 cells was inhibited more than that of the CHO cells, with respect to the controls. A statistically significant inhibitory effect was observed for the invasive MDA-MB-231 cell line (Figure 10).

NAMI-A and the micelles display cell type specificity, characterized by a more pronounced effect on tumor cells, than on the nontumorigenic CHO cells. The NAMI-A micelles did not display any statistically significant effect for the migration assay, although they had a more pronounced inhibitory effect than NAMI-A. However, since the NAMI-A micelles significantly inhibited the invasion of the highly invasive MDA-MB-231 cells, it can be inferred that these drugs also interfere more selectively with tumor cells with the highest inclination to invade and metastasise. Thus, it is probable that

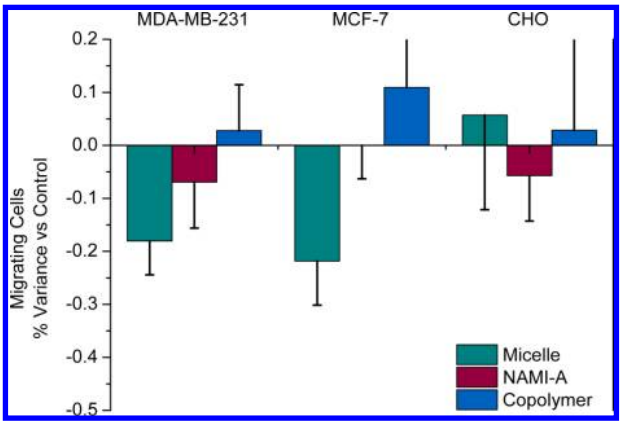

Figure 9. Effect of NAMI-A, PVIm-PPEGMEA, and P(NAMI-A)-PPEGMEA Micelles on the haptotactic migration of cells through polycarbonate filters. MDA-MB-231, MCF-7, and CHO cell were treated for 1 h with the drugs where [Ru] = 5 μM. The cells were then removed from the flasks, collected, resuspended and seeded on the insets of Transwell cell culture chambers. Data represent cells that after 24 h have migrated and are present on the lower surface of the filter. Data are the percent of variation vs controls calculated from the mean ± SD of one experiment performed in triplicate.

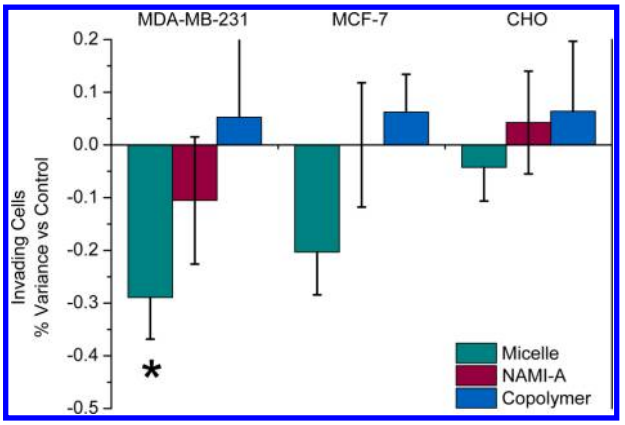

Figure 10. Effect of NAMI-A, PVIm-PPEGMEA, and P(NAMI-A)-PPEGMEA Micelles on the invasion of cells through Matrigel. MDA-MB-231, MCF-7, and CHO cells were treated for 1 h with the drugs where [Ru] = 5 μM. The cells were then removed from the flasks, collected, resuspended and seeded on inserts. Data represent cells that after 96 h have invaded and are present on the lower surface of the filter. Data are the percent of variation vs controls calculated from the mean ± SD of one experiment performed in triplicate. Key: (*) significant difference vs control, $p < 0.05$.

the antimetastatic ability of NAMI-A has been enhanced by incorporation in polymeric nanoparticles. It would be valuable to evaluate the antimetastatic potential of these nanoparticles at a higher ruthenium concentration and also *in vivo*.

CONCLUSIONS

An amphiphilic block copolymer capable of self-assembling into polymeric micelles was identified as an appropriate drug carrier for NAMI-A. A suitable method for the synthesis of a macromolecular NAMI-A drug was identified—the polymerization of vinyl imidazole and subsequent addition of a ruthenium(III) precursor complex. A water-soluble block copolymer was designed to increase biocompatibility and cell uptake through the formation of micelles. On average, across the tested cell lines, a 1.5 times increase in toxicity was found

dx.doi.org/10.1021/ma402078d | *Macromolecules* XXXX, XXX, XXX–XXX

for the NAMI-A block copolymer micelles when compared to the NAMI-A molecule. Furthermore, the micelles were shown to have an improved antimetastatic potential than NAMI-A. Further work will entail a detailed assessment of the antimetastatic effects of the macromolecular NAMI-A chemotherapeutic *in vivo*.

■ ASSOCIATED CONTENT

Supporting Information

Schemes showing the synthesis and polymerization of VIm and the synthesis of the Ru precursor, figures showing NMR spectra, SEC traces, and the viablility of cells, and tables of crystallographic and reaction data. This material is available free of charge via the Internet at http://pubs.acs.org.

■ AUTHOR INFORMATION

Corresponding Author

*(M.H.S.) E-mail: M.stenzel@unsw.edu.au. Fax: +61-2-93856250. Telephone: +61-93854344.

Notes

The authors declare no competing financial interest.

■ ACKNOWLEDGMENTS

We would like to thank Dr. Andrew Gregory for preparing the RAFT Agent, Dr. Mohan Bhadbhade at the Solid State and Elemental Analysis Unit, UNSW, for the X-ray crystallography analysis of the complexes and The Campbell Microanalytical Laboratory at the University of Otago in New Zealand for the solid-state elemental analysis of the polymer.

■ REFERENCES

(1) Dyson, P. J.; Sava, G. *Dalton Trans.* **2006**, *35*, 1929−33.
(2) Morris, R. R. E.; Aird, R. E.; del Socorro Murdoch, P.; Chen, H.; Cummings, J.; Hughes, N. D.; Parsons, S.; Parkin, A.; Boyd, G.; Jodrell, D. I.; Sadler, P. J. *J. Med. Chem.* **2001**, *44*, 3616−21.
(3) Antonarakis, E. S.; Emadi, A. *Cancer Chemother. Pharm.* **2010**, *66*, 1−9.
(4) Allardyce, C. S.; Dyson, P. J. *Platinum Met. Rev.* **2001**, *45*, 62−9.
(5) Sava, G.; Capozzi, I.; Clerici, K.; Gagliardi, G.; Alessio, E.; Mestroni, G. *Clin. Exp. Metastasis* **1998**, *16*, 371−9.
(6) Bergamo, A.; Gaiddon, C.; Schellens, J. H. M.; Beijnen, J. H.; Sava, G. *J. Inorg. Biochem.* **2012**, *106*, 90−9.
(7) Kostova, I. *Curr. Med. Chem.* **2006**, *13*, 1085−1107.
(8) Groessl, M.; Hartinger, C. G.; Dyson, P. J.; Keppler, B. K. *J. Inorg. Biochem.* **2008**, *102*, 1060−5.
(9) Huynh, V. T.; Quek, J. Y.; de Souza, P. L.; Stenzel, M. H. *Biomacromolecules* **2012**, *13*, 1010−23.
(10) Pearson, S.; Scarano, W.; Stenzel, M. H. *Chem. Commun. (Cambridge, U.K.)* **2012**, *48*, 4695−7.
(11) Blunden, B. M.; Thomas, D. S.; Stenzel, M. H. *Polym. Chem.* **2012**, *3*, 2964−75.
(12) Blunden, B. M.; Lu, H.; Stenzel, M. H. *Biomacromolecules* **2013**, *14*, 4177−88.
(13) Savić, R.; Eisenberg, A.; Maysinger, D. *J. Drug Target* **2006**, *14*, 343−55.
(14) Stenzel, M. H. *Chem. Commun. (Cambridge, U.K.)* **2008**, *44*, 3486−503.
(15) Matsumura, Y.; Maeda, H. *Cancer Res.* **1986**, *46*, 6387−92.
(16) Ambade, A. V.; Savariar, E. N.; Thayumanavan, S. *Mol. Pharmaceutics* **2005**, *2*, 264−72.
(17) Mikhail, A. S.; Allen, C. *Biomacromolecules* **2010**, *11*, 1273−80.
(18) Cabral, H.; Nishiyama, N.; Okazaki, S.; Koyama, H.; Kataoka, K. *J. Controlled Release* **2005**, *101*, 223−32.
(19) Cabral, H.; Nishiyama, N.; Kataoka, K. *J. Controlled Release* **2007**, *121*, 146−55.
(20) Nishiyama, N.; Yokoyama, M.; Aoyagi, T.; Okano, T.; Sakurai, Y.; Kataoka, K. *Langmuir* **1999**, *15*, 377−83.
(21) Nishiyama, N.; Kataoka, K. *J. Controlled Release* **2001**, *74*, 83−94.
(22) Nishiyama, N.; Okazaki, S.; Cabral, H.; Miyamoto, M.; Kato, Y.; Sugiyama, Y.; Nishio, K.; Matsumura, Y.; Kataoka, K. *Cancer Res.* **2003**, *63*, 8977−83.
(23) Bontha, S.; Kabanov, A. V.; Bronich, T. K. *J. Controlled Release* **2006**, *114*, 163−74.
(24) Matsumoto, A.; Matsukawa, Y.; Suzuki, T.; Yoshino, H. *J. Controlled Release* **2005**, *106*, 172−80.
(25) Anderson, E. B.; Long, T. E. *Polymer* **2010**, *51*, 2447−54.
(26) Hakamatani, T.; Asayama, S.; Kawakami, H. *Nucleic Acids Symp. Ser.* **2008**, *52*, 677−8.
(27) Srivastava, A.; Waite, J. H.; Stucky, G. D.; Mikhailovsky, A. *Macromolecules* **2009**, *42*, 2168−76.
(28) Asayama, S.; Sekine, T.; Kawakami, H.; Nagaoka, S. *Bioconjugate Chem.* **2007**, *18*, 1662−7.
(29) Green, M. D.; Allen, M. H.; Dennis, J. M.; La Cruz, D. S.; Gao, R.; Winey, K. I.; Long, T. E. *Eur. Polym. J.* **2011**, *47*, 486−96.
(30) Pekel, N.; Gu, O. *Colloid Polym. Sci.* **1999**, *573*, 570−3.
(31) Yuan, J.; Schlaad, H.; Giordano, C.; Antonietti, M. *Eur. Polym. J.* **2011**, *47*, 772−81.
(32) Allen, M. H.; Hemp, S. T.; Smith, A. E.; Long, T. E. *Macromolecules* **2012**, *45*, 3669−76.
(33) Skey, J.; O'Reilly, R. K. *Chem. Commun. (Cambridge, U.K.)* **2008**, *44*, 4183−5.
(34) Piotto, M.; Saudek, V.; Sklenář, V. *J. Biomol. NMR* **1992**, *2*, 661−5.
(35) Alessio, E.; Balducci, G.; Lutman, A.; Mestroni, G.; Calligaris, M.; Attia, W. M. *Inorg. Chim. Acta* **1993**, *203*, 205−17.
(36) Alessio, E.; Balducci, G.; Calligaris, M.; Costa, G.; Attia, W. M.; Mestroni, G. *Inorg. Chem.* **1991**, *30*, 609−18.
(37) Mestroni, G.; Alessio, E.; Sava, G. Salts of anionic complexes of RU (III), as antimetastatic and antineoplastic agents. US006221905B1, 2001.
(38) Bergamo, A.; Masi, A.; Dyson, P. J.; Sava, G. *Int. J. Oncol.* **2008**, *33*, 1281−1289.
(39) Barz, M.; Luxenhofer, R.; Zentel, R.; Kabanov, A. V. *Biomaterials* **2009**, *30*, 5682−90.
(40) Panich, A. M.; Furman, G. B. *Diamond Relat. Mater.* **2012**, *23*, 157−161.
(41) Lv, H.; Zhang, S.; Wang, B.; Cui, S.; Yan, J. *J. Controlled Release* **2006**, *114*, 100−9.
(42) Zhang, L.; Nguyen, T. L. U.; Bernard, J.; Davis, T. P.; Barner-Kowollik, C.; Stenzel, M. H. *Biomacromolecules* **2007**, *8*, 2890−901.
(43) Groessl, M.; Zava, O.; Dyson, P. J. *Metallomics* **2011**, *3*, 591−9.
(44) Alessio, E.; Mestroni, G.; Bergamo, A.; Sava, G. *Curr. Top. Med. Chem.* **2004**, *4*, 1525−35.
(45) Bratsos, I.; Jedner, S.; Gianferrara, T.; Alessio, E. *Chimia (Aarau)* **2007**, *61*, 692−7.
(46) Bergamo, A.; Gagliardi, R.; Scarcia, V.; Furlani, A.; Alessio, E.; Mestroni, G.; Sava, G.; Foundation, C.; Sciences, B. *J. Pharm. Exp. Ther.* **1999**, *289*, 559−64.